Article

Enhancement of photocatalytic properties of Ga₂O₃-SiO₂ nanoparticles by Pt deposition

E. S. BAEISSA [a] , R. M. MOHAMED [a,b,c,*]

[a] Chemistry Department, Faculty of Science, King Abdulaziz University, P.O. Box: 80203, Jeddah 21589, Saudi Arabia
[b] Advanced Materials Department, Central Metallurgical R&D Institute, CMRDI, P.O. Box 87, Helwan, Cairo, Egypt
[c] Center of Excellence in Environmental Studies, King Abdulaziz University, P.O. Box 80216, Jeddah 21589, Saudi Arabia

ARTICLE INFO

ABSTRACT

Ga₂O₃-SiO₂ nanoparticles were prepared by a sol-gel method and Pt was then immobilized on their surface via photo-assisted deposition (PAD). The produced samples were characterized using X-ray diffraction (XRD), ultraviolet and visible spectroscopy, photoluminescence emission spectroscopy, and surface area measurements. The catalytic performances of the Ga₂O₃-SiO₂ and Pt/ Ga₂O₃-SiO₂ samples were evaluated for the degradation of cyanide using visible light. XRD and EDX results showed that the Pt was well dispersed within the Ga₂O₃-SiO₂ phase and was detected on the surface of the catalyst, which confirmed the successful loading of Pt ions by the PAD method. BET results revealed that the surface area of Ga₂O₃-SiO₂ was higher than that of Pt/Ga₂O₃-SiO₂. 0.3 wt% Pt/Ga₂O₃-SiO₂ exhibited the highest photocatalytic activity for degradation of cyanide under visible light. The catalyst could be reused with no loss in activity for the first 10 cycles.

1. Introduction

Environmental problems associated with hazardous wastes and toxic water pollutants have attracted much attention. Cyanides are one of the major groups of toxins found in wastewaters produced by various industries, including metal cleaning, plating, electroplating, metal processing, automobile parts manufacturing, steel tempering, mining, photography, pharmaceuticals, coal coking, ore leaching, and plastics. Among various physical, chemical, and biological techniques for wastewater treatment, photocatalysis is considered a cost-effective process for water remediation [1–3].

Advanced oxidation processes (AOPs) generate hydroxyl radicals for the oxidative degradation of organic pollutants to CO₂ and water. Photocatalytic oxidation using TiO₂ has been widely studied by many researchers [4,5]. Despite its positive attributes, the main drawback associated with TiO₂ semicon-ductor photocatalysts is charge carrier recombination [6]. Gallium oxide has been reported as a water splitting photocatalyst for the generation of hydrogen gas. β-Ga₂O₃ is a wide band gap semiconductor that finds versatile applications in optoelectronic devices, high temperature electronic devices, and high temperature stable gas sensors [7–9]. It has recently been reported that nanophases of gallium oxide can be used as an efficient photocatalyst for the oxidative degradation of organic effluents [10–16].

The main drawback associated with β-Ga₂O₃ photocatalysts is their UV-only absorption and low surface area. Therefore, the main research goals are to increase the surface area of β-Ga₂O₃ by loading onto inert supports such as SiO₂ and Al₂O₃ and to convert its absorption from UV to visible light by metal doping.

There are as yet no reports of the degradation of cyanide in aqueous solution using gallium oxide. The present study aims

to synthesize and characterize Pt/β-Ga$_2$O$_3$-SiO$_2$ and evaluate its photocatalytic activity for the oxidative degradation of cyanide in aqueous phase under visible light.

2. Experimental

2.1. Preparation

0.2 Ga$_2$O$_3$:1 SiO$_2$ nanoparticles were prepared using a sol-ge method. Tetraethylorthosilicate (TEOS; 98% purity, Acros; 20 ml) was mixed with ethyl alcohol (absolute, Aldrich), ultra pure water, and nitric acid (Aldrich) as catalyst under magnetic stirring for 60 min. Then, the calculated amount of gallium isoperoxide (GP; Ga(OC$_3$H$_7$)$_3$, Aldrich) was added slowly to the previous mixture with continuous stirring, which was continued for a further 60 min. The prepared sol was left to stand to allow gel formation. The gel sample was calcined at 550 °C for 5 h in air to obtain a Ga$_2$O$_3$-SiO$_2$ xerogel.

Pt/Ga$_2$O$_3$-SiO$_2$ catalysts (0.1, 0.2, 0.3, and 0.4 wt% Pt metal) were produced using a photo-assisted deposition (PAD) method as follows. Pt metal was deposited on the Ga$_2$O$_3$-SiO$_2$ sample from an aqueous solution of chloroplatinic acid (H$_2$PtCl$_6$, Sigma-Aldrich) under UV irradiation. The samples were dried at 105 °C and then reduced under H$_2$ (20 ml/min) at 673 °C for 2 h.

2.2. Characterization

X-ray diffraction (XRD) analysis was carried out at room temperature using a Bruker axis D8 with Cu K_α radiation (λ = 0.1540 nm) over a 2θ collection range of 10°–80°. Specific surface area was calculated from measurements of N$_2$-adsorption using a Nova 2000 series Chromatech apparatus at –196 °C. All samples were treated under vacuum at 200 °C for 2 h prior to the measurements. The band gaps of the samples were measured by UV-Vis diffuse reflectance spectroscopy in air at room temperature within a wavelength range of 200–800 nm using a UV/Vis/NIR spectrophotometer (V-570, JASCO, Japan). Transmission electron microscopy (TEM) was performed with a JEOL-JEM-1230 microscope. The samples were prepared for imaging by dispersion in ethanol followed by ultrasonication for 30 min, after which a small amount of the resulting suspension was dropped onto a carbon-coated copper grid and dried before the sample was loaded into the TEM. Photoluminescence (PL) emission spectra were recorded with a Shimadzu RF-5301 fluorescence spectrophotometer.

2.3. Catalytic activity test

The application of the synthesized nanocomposite to the photodegradation of cyanide was investigated under visible light. Experiments were carried out using a horizontal cylinder annular batch reactor. The photocatalyst was irradiated with a blue fluorescent lamp (150 W) doubly covered with a UV cut-off filter. The intensity data of the UV light were confirmed to be under the detection limit (0.1 mW/cm^2) of a UV radiometer. In a typical experiment, the chosen weight of catalyst was

suspended in 300 ml of 100 mg/L potassium cyanide (KCN) solution, which had been adjusted to pH 10.5 using ammonia solution to avoid the evolution of HCN gas. The reaction was carried out isothermally at 25 °C and samples of the reaction mixture were taken at different intervals over a total reaction time of 1 h. The CN$^-$$_{(aq)}$ concentration of the samples was estimated by volumetric titration with AgNO$_3$, using potassium iodide to determine the titration end-point [17]. The removal efficiency of CN$^-$$_{(aq)}$ was measured by applying the following equation:

$$\text{Removal efficiency (\%)} = (C_0 - C) / C_0 \times 100$$

where C_0 is the initial concentration of uncomplexed CN$^-$$_{(aq)}$ in solution, and C is the concentration of unoxidized CN$^-$$_{(aq)}$ in solution.

3. Results and discussion

3.1. Structural, morphological, and compositional characterization results

The XRD patterns of the as-prepared Ga$_2$O$_3$-SiO$_2$ and Pt/Ga$_2$O$_3$-SiO$_2$ nanoparticles prepared by PAD are compared in Fig. 1. Both samples were mainly composed of monoclinic β-Ga$_2$O$_3$ with lattice constants a = 1.224 nm, b = 0.304 nm, c = 0.581 nm, and β = 103.80, which are in good agreement with the reported values of β-Ga$_2$O$_3$ (JCPDS 41-1103), which indicated that the β-Ga$_2$O$_3$ structure remained after the photo-assisted deposition of Pt. However, no diffraction peaks assignable to Pt appeared in the patterns of the Pt/Ga$_2$O$_3$-SiO$_2$ samples. This was probably because of the low Pt doping content used. Moreover, the data may imply that the Pt was well dispersed within the Ga$_2$O$_3$-SiO$_2$ phase.

The results of EDX analysis, which identifies only the surface elements of a sample, are shown in Fig. 2. A signal attributable to the presence of Pt on the surface of the catalyst was detected, which confirmed the successful loading of Pt ions using the PAD method.

TEM images of the Pt/Ga$_2$O$_3$-SiO$_2$ nanoparticles are shown in Fig. 3. The images show that Pt ions were dispersed on the surface of the catalyst and that their diameter increased with
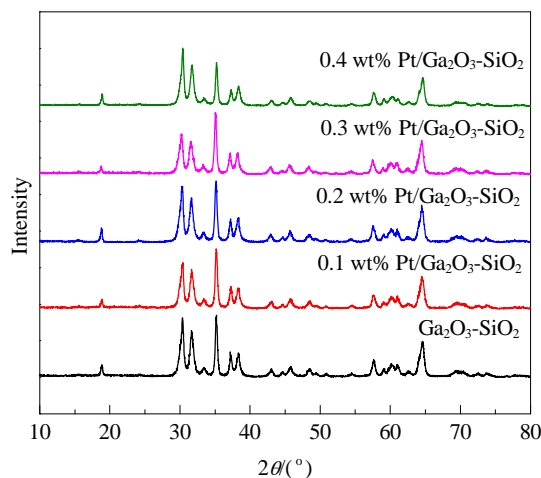

Fig. 1. XRD patterns of Ga$_2$O$_3$-SiO$_2$ and Pt/Ga$_2$O-SiO$_2$ nanoparticles.
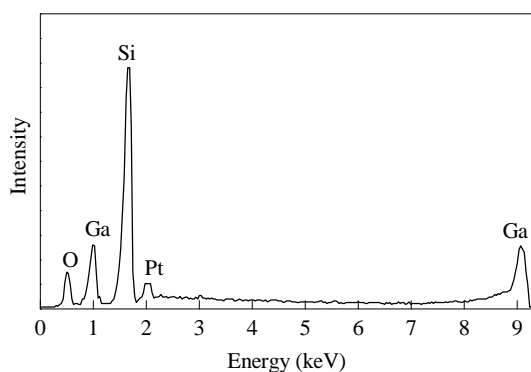
Fig. 2. EDX analysis result for 0.3 wt%Pt/Ga$_2$O-SiO$_2$.

the content of Pt. It is clear that the homogeneity of the Pt increased with the amount of Pt ions up to 0.3 wt%. At higher concentration of Pt ions i.e., 0.4 wt%, the homogeneity of the Pt decreased. This observation indicated that there was an optimum value for the deposition of Pt ion.

3.2. Surface area analysis

The specific surface area (A_{BET}) of the Ga$_2$O$_3$-SiO$_2$ and Pt/Ga$_2$O$_3$-SiO$_2$ nanoparticles were determined to be 400, 393, 360, 349, and 341 m^2/g for the Ga$_2$O$_3$-SiO$_2$, 0.1 wt% Pt/Ga$_2$O$_3$-SiO$_2$, 0.2 wt% Pt/Ga$_2$O$_3$-SiO$_2$, 0.3 wt% Pt/Ga$_2$O$_3$-SiO$_2$, and 0.4 wt% Pt/Ga$_2$O$_3$-SiO$_2$, respectively. The surface area values and the data calculated from the t-plots are collected in Table 1. Furthermore, the total pore volume of the as-prepared Ga$_2$O$_3$-SiO$_2$ was found to be higher than that of the Pt/Ga$_2$O$_3$-SiO$_2$ samples because of the blocking of some pores by the deposition of Pt metal. The A_{BET} and A_t values were generally close for most samples, indicating the presence of mesopores.
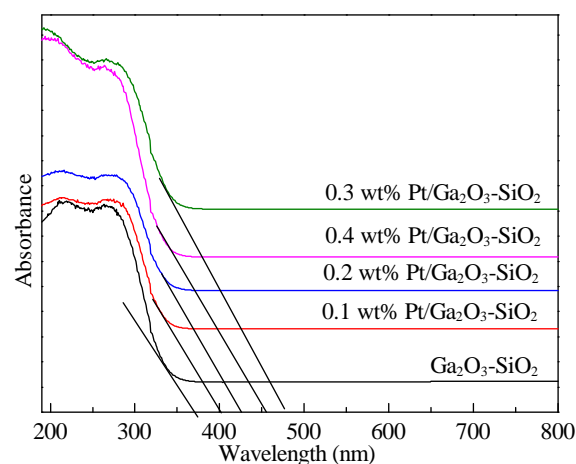

Fig. 4. Diffuse reflectance UV-Vis absorption spectra of Ga$_2$O$_3$-SiO$_2$ and Pt/Ga$_2$O-SiO$_2$ nanoparticles.

3.3. Optical characterization

The UV-Vis diffuse reflectance spectra of the Ga$_2$O$_3$-SiO$_2$ and Pt/Ga$_2$O$_3$-SiO$_2$ nanoparticles are displayed in Fig. 4. The loading of Pt ions caused a red shift toward higher wavelength from 383 to 448 nm for different Pt loadings compared with that of the as-prepared Ga$_2$O$_3$-SiO$_2$, which had a wavelength of about 357 nm. The direct band gap energies of the Ga$_2$O$_3$-SiO$_2$ and Pt/Ga$_2$O$_3$-SiO$_2$ were calculated from their reflection spectra based on a method suggested by Kumar et al. [18], and the results are presented in Table 2. It is clear that the energy gap decreased with increase in Pt ion loading up to 0.3 wt%. At higher Pt ion concentration, i.e., 0.4 wt%, the band gap increased again. This observation indicated that there was an optimum amount of Pt loading.

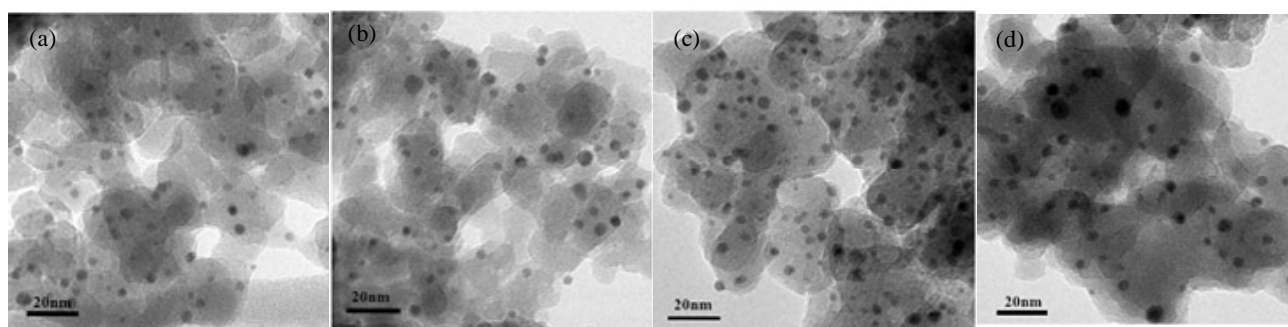PL emission spectra were used to study the transfer of

Fig. 3. TEM images of Pt/Ga$_2$O$_3$-SiO$_2$ nanoparticles. Pt content (wt%): (a) 0.1; (b) 0.2; (c) 0.3; (d) 0.4.

Table 1

Texture parameters of Ga$_2$O$_3$-SiO$_2$ and Pt/ Ga$_2$O$_3$-SiO$_2$ nanoparticles.

Sample	Surface area (m^2/g)					Pore volume (cm^3/g)			Mean pore radius (nm)
	BET	t-plot	Micropores	Mesopores	External	Total	Micropores	Mesopores	
Ga$_2$O$_3$-SiO$_2$	400	417	323	264	77	0.890	0.080	0.810	3.6
0.1 wt% Pt/Ga$_2$O$_3$-SiO$_2$	393	410	325	259	68	0.790	0.070	0.730	3.8
0.2 wt% Pt/Ga$_2$O$_3$-SiO$_2$	360	375	300	238	60	0.720	0.060	0.660	3.9
0.3 wt% Pt/Ga$_2$O$_3$-SiO$_2$	349	364	299	230	58	0.700	0.055	0.648	4.0
0.4 wt% Pt/Ga$_2$O$_3$-SiO$_2$	341	355	295	225	46	0.690	0.050	0.640	4.1

Table 2
Band gap energy of Ga$_2$O$_3$-SiO$_2$ and Pt/ Ga$_2$O$_3$-SiO$_2$ nanoparticles.

Sample	Band gap energy (eV)
Ga$_2$O$_3$-SiO$_2$	3.47
0.1 wt% Pt/Ga$_2$O$_3$-SiO$_2$	3.24
0.2 wt% Pt/Ga$_2$O$_3$-SiO$_2$	3.00
0.3 wt% Pt/Ga$_2$O$_3$-SiO$_2$	2.77
0.4 wt% Pt/Ga$_2$O$_3$-SiO$_2$	2.92

photogenerated electrons and holes and understand the separation and recombination of photogenerated charge carriers in the samples. To investigate the photoelectric properties of the prepared samples, PL spectra were measured for samples excited at 265 nm at room temperature, as shown in Fig. 5. It is clear that the position of the PL emission of Ga$_2$O$_3$-SiO$_2$ was different from those of the Pt/Ga$_2$O$_3$-SiO$_2$ samples, and PL intensity greatly decreased with the increase of Pt loading up to 0.3 wt%. At higher Pt ion concentration, i.e. 0.4 wt%, the PL intensity increased again, in agreement with the UV-Vis results. Deposited Pt particles act as trapping sites to capture photogenerated electrons from the conduction band, thereby separating the photogenerated electron-hole pairs. It is generally accepted that the incorporation of noble metal nanoparticles into semiconductor-based catalysts is able to enhance the light absorption of the catalyst in the visible-light region. This leads to a shift of the absorption edge of the catalyst toward longer wavelengths, indicating a decrease in the band gap energy and an increase in the amount of photogenerated electrons and holes available to participate in photocatalytic reactions. In the present case, Pt seems to modify the interface of Ga$_2$O$_3$-SiO$_2$ in a way that alters the mechanisms by which photogenerated charge carriers undergo recombination or surface reactions. This would force the Ga$_2$O$_3$-SiO$_2$ mixed oxide to be activated in the visible region. The observed shift in emission position could therefore be attributed to charge transfer between the Pt generated band and the conduction band of the Ga$_2$O$_3$-SiO$_2$ semiconductor.
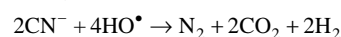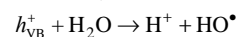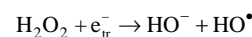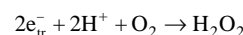
3.4. Photocatalytic activities

In general, the process of semiconductor photocatalysis begins with the direct absorption of supra-band gap photons and the resulting generation of electron-hole pairs in the semiconductor particles. This is followed by diffusion of the charge carriers to the surface of the particle. The photocatalytic reactions can be listed as follows.
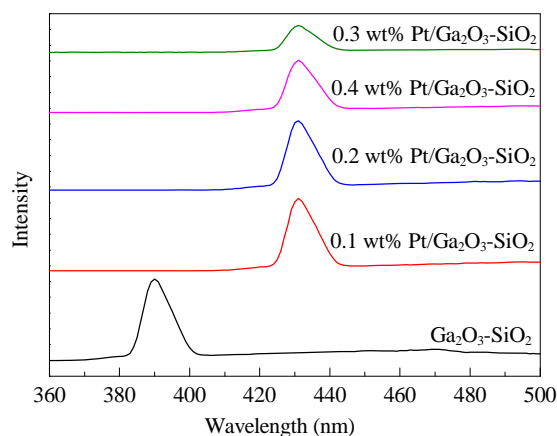
$$Ga_2O_3 + h\upsilon \rightarrow e^-_{CB} + h^+_{VB}$$
$$e^-_{CB}(Pt) \rightarrow e^-_{tr}(Pt)$$
$$e^-_{tr} + O_2(ads) \rightarrow O^-_2$$
$$2e^-_{tr} + 2H^+ + O_2 \rightarrow H_2O_2$$
$$H_2O_2 + e^-_{tr} \rightarrow HO^- + HO^\bullet$$
$$h^+_{VB} + H_2O \rightarrow H^+ + HO^\bullet$$
$$2CN^- + 4HO^\bullet \rightarrow N_2 + 2CO_2 + 2H_2$$
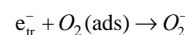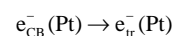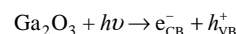
Photocatalytic activity is believed to be associated with the generation of highly reactive peroxide (O^-_2) and hydroxyl radical (HO$^\bullet$) species by electrons and holes reacting with water at the surface of the semiconductor. If surface defect states exist, they may be able to trap electrons or holes. This prevents recombination and the rate of oxidation-reduction reactions may be increased as a result. In our case, Pt acted as an electron trap and the rate of photocatalytic activity increased. Photocatalytic activity is known to be dependent on crystallinity, surface area, and morphology, and may be improved by slowing the recombination of photogenerated electron-hole pairs, extending the excitation wavelength to a lower energy range, and increasing the amount of surface-adsorbed reactant species.

Figure 6 shows the results of the photocatalytic degradation of aqueous cyanide using Ga$_2$O$_3$-SiO$_2$ catalysts with different amount of Pt under visible light. The experiment was carried out under the following conditions: solution pH 10.5, 300 ml 100 ppm KCN solution, and 0.20 g catalyst. The results indicate that Ga$_2$O$_3$-SiO$_2$ and 0.1 wt% Pt/Ga$_2$O$_3$-SiO$_2$ had almost no photocatalytic activity under visible light because of their absorbance in the UV region only. An increase of deposited Pt amount from 0.2 to 0.3 wt% led to high cyanide removal efficiencies of 55% and 100%, respectively. However, further increase of Pt amount above 0.3 wt% slightly decreased cyanide removal efficiency to 88%.

The reaction order with respect to cyanide for the Ga$_2$O$_3$-SiO$_2$ and Pt/Ga$_2$O$_3$-SiO$_2$ samples was determined by

Fig. 5. PL spectra of Ga$_2$O$_3$-SiO$_2$ and Pt/Ga$_2$O-SiO$_2$ nanoparticles.
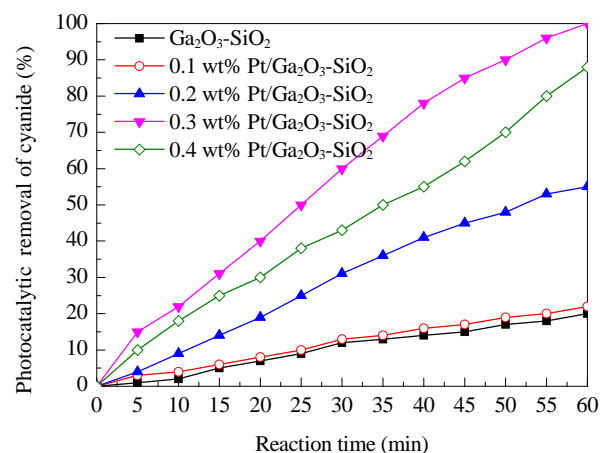
Fig. 6. Effect of Pt content on photocatalytic activity of Ga$_2$O$_3$-SiO$_2$ for cyanide removal.

Table 3

Rate constant of reaction kinetic of cyanide with Ga_2O_3-SiO_2 and Pt/Ga_2O_3-SiO_2 samples.

Sample	$k \times 10^{-4}$ (min^{-1})
Ga_2O_3-SiO_2	10
0.1 wt% Pt/Ga_2O_3-SiO_2	10
0.2 wt% Pt/Ga_2O_3-SiO_2	50
0.3 wt% Pt/Ga_2O_3-SiO_2	160
0.4 wt% Pt/Ga_2O_3-SiO_2	90

Table 4

Rate constant of reaction kinetic of cyanide with different loading of 0.3 wt% Pt/Ga_2O_3-SiO_2 sample.

Loading (g)	$k \times 10^{-4}$ (min^{-1})
0.10	120
0.15	130
0.20	160
0.25	170
0.30	240
0.35	250

plotting reaction time versus log[cyanide] according to the following equation.

$$\text{Log}[C]_t = -kt + \text{Log}[C]_0$$

where $[C]_0$ and $[C]_t$ represent the concentration of the substrate in solution at zero time and t time of illumination, respectively, and k represents the apparent rate constant (min^{-1}).
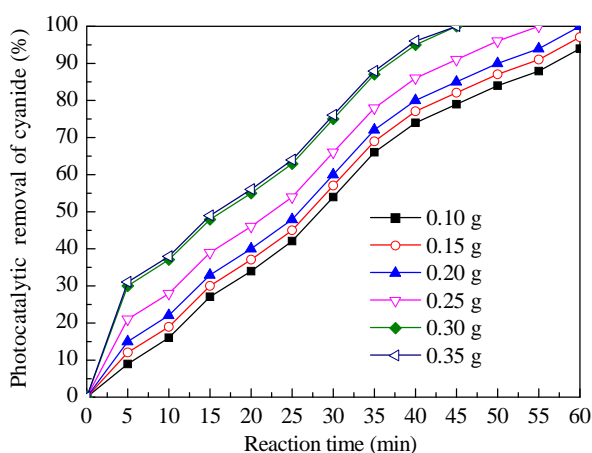
The apparent rate constants are summarized in Table 3. The results show that the reaction followed first order kinetics with respect to cyanide and that the rate constants were in the range of $10–160 \times 10^{-4}$ min^{-1}. The first order rate equation for cyanide is given by $R = k$ [cyanide].

Figure 7 shows the results of the photocatalytic degradation of cyanide solution using Ga_2O_3-SiO_2 catalysts with different catalyst loading under visible light. The experiment was carried out under the following conditions: solution pH 10.5, 300 ml 100 ppm KCN solution, and 0.3 wt% Pt/Ga_2O_3-SiO_2. The results indicate that increased catalyst loading from 0.10 to 0.20 g increased cyanide removal efficiency from 94% to 100% after 60 min reaction time. However, further increased catalyst loading from 0.20 to 0.30 g decreased the reaction time from 60 to 45 min. Above 0.30 g, catalyst loading had no significant effect on cyanide removal efficiency or reaction time. Therefore, the optimum catalyst loading was found to be 0.30 g.

The reaction order with respect to cyanide was for different catalyst loadings determined by plotting reaction time versus log[cyanide] according to the following equation.

$$\text{Log}[C]_t = -kt + \text{Log}[C]_0$$

where $[C]_0$ and $[C]_t$ represent the concentration of the substrate in solution at zero time and t time of illumination, respectively, and k represents the apparent rate constant (min^{-1}).

The apparent rate constants are summarized in Table 4. The results show that the reaction followed first order kinetics with respect to cyanide and that the rate constants were in the range of $120–240 \times 10^{-4}$ min^{-1}. The first order rate equation for cyanide is given by $R = k$ [cyanide].

The photocatalyst was then used to photodegrade cyanide repeatedly under visible irradiation. The photocatalytic performance was 100% during the first 10 cycles, after which the photocatalytic activity of the recycled photocatalyst decreased by 5% after 10 cycles. This result shows that the recovery of the photocatalyst was effective and the repeatability of the photocatalytic activity of the Pt/Ga_2O_3-SiO_2 was promising.

4. Conclusions

A Pt/Ga_2O_3-SiO_2 photocatalyst was successfully synthesized and proven to be a promising catalyst because of its high removal efficiency of the chosen pollutant under visible light. The red shift phenomenon observed in the UV-Vis spectra of the Pt/Ga_2O_3-SiO_2 samples compared with that of as-prepared Ga_2O_3-SiO_2 was found to depend on the amount of Pt deposited. The results of the photocatalytic degradation of aqueous cyanide solution showed that Pt/Ga_2O_3-SiO_2 nanoparticles with 0.3 wt% Pt exhibited the highest catalytic activity and efficiency for water purification and thus may find potential application in related fields. The catalyst could be reused with no loss in activity during the first 10 cycles. The cyanide degradation efficiency of was still high, around 95%, after the 11th use of the photocatalyst.

Fig. 7. Effect of loading of 0.3 wt% Pt/Ga_2O_3-SiO_2 on photocatalytic removal of cyanide.

References

[1] Paola A D, García-López E, Marcì G, Palmisano L. *J Hazard Mater*, 2012, 211–212: 3
[2] Li Y, Li J H, Chen S S, Diao W H. *Environ Pollut*, 2012, 165: 77
[3] Robertson P K J, Robertson J M C, Bahnemann D W. *J Hazard Mater*, 2012, 211–212: 161
[4] Andreozzi R, Caprio V, Insola A, Marotta R. *Catal Today*, 1999, 53: 51
[5] Hoffmann R M, Martin T S, Choi W, Bahneman W D. *Chem Rev*,

Graphical Abstract

Enhancement of photocatalytic properties of Ga₂O₃-SiO₂ nanoparticles by Pt deposition

E. S. BAEISSA, R. M. MOHAMED*
King Abdulaziz University, Saudi Arabia
Central Metallurgical R&D Institute, CMRDI, Egypt

Pt/Ga₂O₃-SiO₂ photocatalyst is able to degrade aqueous waste materials under visible light.
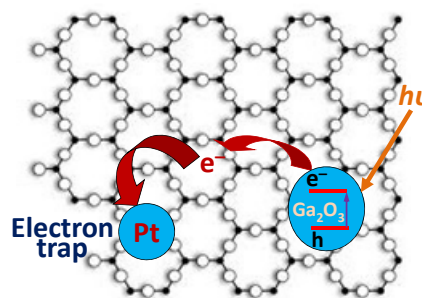
1995, 95: 69

[6] Mills A, Hunte S L. *J Photochem Photobiol A*, 1997, 108: 1

[7] Lin J, Yu M, Lin C K, Liu X M. *J Phys Chem C*, 2007, 111: 5835

[8] Dai Z R, Pan Z W, Wang Z L. *Adv Funct Mater*, 2003, 13: 9

[9] Li Y X, Trinchi A, Wlodarski W, Galatsis K, Kalantar-zadeh K. *Sens Actuators B*, 2003, 93: 431

[10] Hou Y D, Zhang J S, Ding Z X, Wu L. *Powder Technol*, 2010, 203: 440

[11] Hou Y D, Wang X C, Wu L, Ding Z X, Fu X Z. *Envi Sci Technol*, 2006, 40: 5799

[12] Hou Y D, Wu L, Wang X C, Ding Z X, Li Z H, Fu X Z. *J Catal*, 2007, 250: 12

[13] Girija K, Thirumalairajan S, Astam K. P, Mangalaraj D, Ponpandi-anN, Viswanathan C. *Curr Appl Phys*, 2013, 13: 652

[14] Zhao B X, Lü M, Zhou L. *J Environ Sci*, 2012, 24: 774

[15] Zhao W R, Yang Y, Hao R, Liu F F, Wang Y, Tan M, Tang J, Ren D Q, Zhao D Y. *J Hazard Mater*, 2011, 149: 1548

[16] Girija K, Thirumalairajan S, Avadhani G S, Mangalaraj D, Ponpandian N, Viswanathan C. *Mater Res Bull*, in press

[17] Vogel A I, Quantitative Inorganic Analysis, Longmans, London, 1978

[18] Kumar V, Sharma S K, Sharma TP, Singh V. *Opt Mater*, 1999, 12: 115